COMMUNICATION

Check for updates

Lanthanide complexes as molecular dopants for realizing air-stable n-type graphene logic inverters with symmetric transconductance†

Ashwini S. Gajarushi,‡[a] Mohd Wasim,‡[b] Rizwan Nabi,[b] Srinivasu Kancharlapalli,[c] V. Ramgopal Rao,[a] Gopalan Rajaraman, ![ORCID] *[b] Chandramouli Subramaniam ![ORCID] *[b] and Maheswaran Shanmugam ![ORCID] *[b]

An unprecedented air-stable, n-doped graphene field-effect transistor (GFET) with exceptionally enhanced mobility (500%), and concomitantly increased current density ($\sim 10^5$ A cm^{-2}), using lanthanide macrocyclic complexes [Ln(L$_1$)(NO$_3$)$_3$] (where Ln = La (1) or Ce (2)) is demonstrated. Such n-doped GFETs (n-GFETs) exhibit ambient stability for up to 7200 h, attributed to the inherent robustness of 1 and 2. Achieving stable and symmetric n-GFETs is mutually exclusive and elusive, underlining the significance of both high stability and symmetric electron- and hole-currents illustrated here. Interestingly, the influence of C−H···π interaction for the non-covalent charge-transfer between the dopant and GFET is established experimentally for the first time and strongly corroborated through computational investigations. Besides stabilizing n-doped GFETs, the C−H···π interaction unravels a previously unknown direction for electronic tuning of graphene. Importantly, spatial selectivity is achieved through sub-monolayer coverage (0.5–3.0 molecules per μm^2) of the dopants using the femtojet dispensing route. This approach is synergistically combined with the air-stability of n-GFETs to realise complementary, bottom-gated logic inverters exhibiting the highest gain of 0.275 (at 2 V) and lowest power dissipation (~ 30 μW), to realise next-generation molecular electronic devices.

Conceptual insights

We demonstrate an unprecedented route to n-doped graphene through discrete inorganic lanthanide macrocylic complexes for achieving air-stable (>7200 h) graphene field-effect-transistors (GFETs) with symmetric transconductance (8 μS) and high operational current densities (10^5 A cm^{-2}). In contrast to the conventional π···π mechanism of charge-transfer, the lanthanide-macrocyclic complexes exhibit strong C−H···π interactions with graphene, leading to a sharp and stable negative shift in the Dirac point. Such a mechanism of interaction is reported for the first time and is critical to achieve n-doped GFETs. Thus, the practical applicability of such n-doped GFETs is illustrated through a higher-order graphene-based logic inverter providing a voltage gain of 0.275 at 2 V at low power dissipation (~ 30 μW), presenting a paradigm shift over earlier bottom-gated FETs. The exceptional results present a combination of novel materials and approaches that lead to significantly improved results for varied applications ranging from molecular electronics to OLEDs. This study is therefore expected to trigger the exploration of other fundamental supramolecular interactions in controlling the transport properties of GFETs.

Introduction

Engineering electrical transport through monolayered graphene has been a persistent challenge, limiting its application for developing molecular electronic devices.[1] This demands tailoring the Dirac point to achieve ambipolar charge transport in graphene, without compromising its mobility and carrier concentration, aspects challenging to achieve in spite of recent advancements in doping and confinement techniques.[2–6] Alternately, charge-transfer based doping of graphene, predominantly mediated through π–π interactions, provides ease of solution processability and induces minimal structural defects.[7–12] However, poor control over doping density, uniformity and limited stability under ambient conditions restricts practical applicability

[a] Department of Electrical Engineering, Indian Institute of Technology Bombay, Powai, Mumbai-400076, India

[b] Department of Chemistry, Indian Institute of Technology Bombay, Powai, Mumbai-400076, India. E-mail: rajaraman@chem.iitb.ac.in, csubbu@chem.iitb.ac.in, eswar@chem.iitb.ac.in

[c] Theoretical Chemistry Section, Bhabha Atomic Research Centre, Mumbai-400085, India

† Electronic supplementary information (ESI) available: Detailed synthetic procedures, X-ray structural data and their descriptions along with crystallographic and structural parameters, MALDI-ToF, device fabrication details, comparison of GFET performance with other literature reports, thermal stability of 2, performance of n-GFETs under varied environmental conditions, control experiments with GFETs, Raman spectral mapping, X-ray photoelectron spectroscopy and atomic force microscopy of n-doped GFETs and computational studies related to dopant–graphene interaction. CCDC 1849130–1849131. For the ESI and crystallographic data in the CIF or other electronic format see DOI: 10.1039/c8mh01241e

‡ Authors contributed equally to this work.

of such non-covalent doping routes. Even though π–π stacking on graphene is a well-accepted mechanism, the importance of other potential charge-transfer mechanisms such as C–H···π and n–π^* is non-existent in the literature.

In contrast to the organic dopants, discrete inorganic molecules offer excellent air-stability and well-structured molecular energy levels (HOMO and LUMO) and hence are expected to interact strongly with graphene. Despite this advantage and the ease of modulating the C–H···π, n–π^* interactions with graphene, using inorganic dopants has never been investigated. Such systems are expected to provide greater air-stability and superior performance through tuning of energy levels and thus provide access to higher order molecular electronic devices.

In this communication, we demonstrate the use of two, well-defined, air-stable lanthanide macrocyclic complexes $[La(L_1)(NO_3)_3]$ (**1**) and $[Ce(L_1)(NO_3)_3]$ (**2**) (where macrocyclic ligand L_1 = 7,11:20,24-dinitrilodibenzo$[b,m][1,4,12,15]$ tetraazacyclodocosine) that transform pristine GFETs to ambipolar, stable n-GFETs with exceptionally enhanced mobility ($\sim$900 cm^2 V^{-1} s^{-1}) and charge carrier concentration ($\sim 10^{12}$ cm^{-2}). These values achieved on doped GFETs are respectively 500% and 15% higher than undoped GFETs. An innovative approach based on femtojet dispensing enables direct molecular level doping of individual GFETs in a densely packed array using **1** or **2**. Such an approach, employed for the first time, is inspired from biomedical *in vitro* investigations and hence offers distinct advantages over the existing doping technologies.[7–12] The doped GFETs exhibit exceptional ambipolarity (hole-current $\sim$ 800 μA; electron current $\sim$ 700 μA) with symmetric transconductance ($\sim$8 μS) for both electrons and holes, which is extremely scarce in the literature. Furthermore, the doping achieved is invariant for over 7200 h ($\sim$ 10 months) under ambient conditions, attributed to the air-stability of **1** and **2**. The spatial controllability of doping enables the synergistic combination of complementary n-doped and p-doped GFETs at adjacent positions in the same array to realise logic inverters. Such bottom-gate GFET-based inverters exhibit the highest reported gain of 0.275 at a drain voltage (V_{DD}) of 2 V, signifying a 100 times lowering in power dissipation ($\sim$30 μW) compared to the previous reports.[7,10,12,13] Such rectification characteristics obtained by combining molecular-level doping of **1** or **2** with spatial selectivity provide transformative opportunities for realizing next-generation robust electronic devices and logic operators, indicating the superiority of such inorganic-based dopants (**1** and **2**).

Results and discussion

The reaction of one equivalent of $Ln(NO_3)_3 \cdot 6H_2O$ (where Ln = La or Ce) in the presence of two equivalent of 2,6-pyridinedicarboxaldehyde (PC) and *o*-phenylenediamine (PD) in methanolic solution, followed by crystallization in dimethylformamide, results in yellow coloured single crystals (Scheme S1, ESI†). X-ray structure determination reveals the general molecular formula as $[Ln(L_1)(NO_3)_3]$ (where Ln = La (**1**) or Ce (**2**), Fig. 1, Fig. S1, and Tables S1 & S2 of the ESI†). A detailed structural
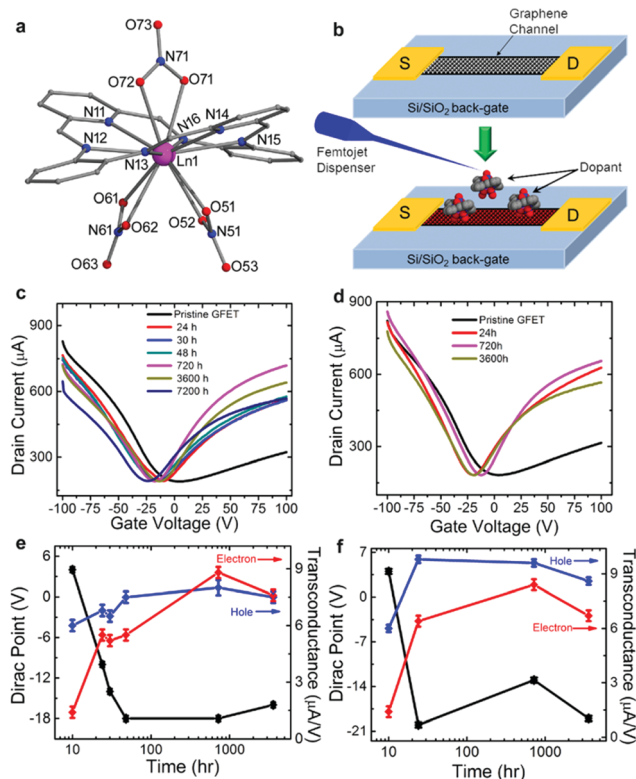

Fig. 1 (a) Representative crystal structure for the molecular dopant **1** or **2**. (b) Schematic representation of back-gated GFET devices and the femtojet based doping route adopted. (c–d) Electrical characteristic of pristine GFETs (black lines), and GFETs doped with **1** and **2**, respectively indicating their doping behaviour and stability. (e and f) Time-dependent variation of the Dirac point and electron–hole transconductance for GFETs upon doping with **1** and **2**, respectively. The error bars are estimated from measurements across 20 n-GFETs.

description of **1** and **2** is given in the ESI.† Both the complexes (**1** and **2**) retain their solid-state structure in solution, as confirmed by Matrix assisted laser desorption ionisation time-of-flight (MALDI-ToF) mass spectrometry (Fig. S2, ESI†).

As reflected from Fig. 1a, the presence of nitrate ligands above and below the plane of L_1 and lack of planarity in L_1 in both **1** and **2** are likely to dictate the nature of molecule–graphene interactions. In order to gain insight into this, the electrical properties of bottom-gated GFETs were investigated (fabrication details in the ESI†). As-fabricated pristine GFETs exhibit p-type behaviour (Dirac point > 0 V, hole mobility $\sim$ 800 cm^2 V^{-1} s^{-1}, electron mobility $\sim$ 200 cm^2 V^{-1} s^{-1}) and low carrier concentration ($\sim 10^{11}$ cm^{-2}) in ambient conditions, compared to pristine GFETs measured under vacuum.[14] Such p-type characteristics originate from the non-specifically adsorbed O_2 and H_2O species on GFETs under ambient conditions.[15] Doping was carried out by dispensing 10^{-12} mL acetonitrile solution of either **1** or **2** (30 μM and 6 μM, respectively) over spatially selected arbitrary locations of pristine GFETs (Fig. 1b). Consequently, a remarkable shift in the Dirac point towards negative gate voltage ($V_g \sim$ −26 V for **1** and −23 V for **2**) along with a concomitant and distinct, irreversible change from unipolar to ambipolar characteristics is observed. The estimated

hole and electron transconductance produced by **1** and **2** (7.5 μS and 7.6 μS for **1** and 8.6 μS and 6.7 μS for **2**, respectively) reveals an ambipolar nature, which is in complete contrast to GFETs before doping (Table S3, ESI†). We note that the stabilisation of the Dirac point occurs ∼10 h after the introduction of dopants on to the GFET surface (Fig. 1e and f). The transfer characteristic measurements (Fig. 1c–f) were carried out on the same devices preserved under ambient conditions over a period of 10 months. The devices are not subjected to any thermal annealing or performance-recovery steps, in contrast to other reports.[7–9,11]

We postulate that the observed scenario is presumably due to the dynamics and timescale of interaction between the dopant and the GFETs to attain the energetically favourable global minimum conformation, which is consistent with the theoretical investigations (*vide infra*). Importantly, the inherent ambient-stability of **1** and **2** is critical to realise stable n-doped GFETs which is further reflected from the invariant transfer characteristics over a duration of 10 months (7200 h, Fig. 1). The stability of n-GFETs achieved here is predominantly due to the large binding energy of **2** on GFETs (−1880 meV) as computed through density functional theory. Such a large binding energy ($E_{binding}$) is at least one order of magnitude higher than other common dopants available under ambient conditions such as O_2 and H_2O (*vide infra*). In addition, the dopants **1** and **2** exhibit excellent thermal stability under ambient conditions (up to ∼350 °C) which presents a substantial improvement in processability over other dopants (Fig. S3, ESI†). Importantly, the invariant characteristics of n-GFETs are further confirmed through measurements carried out under different conditions (thermal stability, relative humidity and time-dependent stability provided in Fig. S4, ESI†). Thus, the observation of a stable Dirac point over a period exceeding 10 months is attributed to the combination of (a) stability of the dopant **2** and (b) unprecedentedly high adsorption energy of **2** on GFETs (*vide infra*). Furthermore, the injection of dopants is carried out through precise femtojet dispensing over a scalable array of isolated GFETs (Fig. 2a and b).

Such simultaneous, stable n-doping and manifestation of ambipolarity under ambient conditions with graphene monolayers overcomes the major challenge of achieving stable n-doped graphene. The ambipolar nature of the n-doped GFETs originates from the synergistic effect of dopant suppression by the bottom-gate configuration employed. This also explains the hysteresis in the transfer characteristics observed, since the bottom-gate configuration is ineffective in screening the effect of ambient humidity from the GFET channel (Fig. S5, ESI†).

The permanent n-doping of the GFETs achieved with **1** or **2**, along with improved and symmetric charge mobility and carrier concentration strongly implies a charge-transfer based noncovalent interaction with graphene. Significantly, the current density measured on our back-gated GFETs (∼10^5 A cm^{-2}) is five orders of magnitude higher as compared to previous reports and is comparable to top-gated hierarchically assembled heterostructured devices.[16–18] Conventionally such interactions are predominantly mediated through π–π stacking with volatile organic dopants,[7–12] leading to poor stability and unreliable
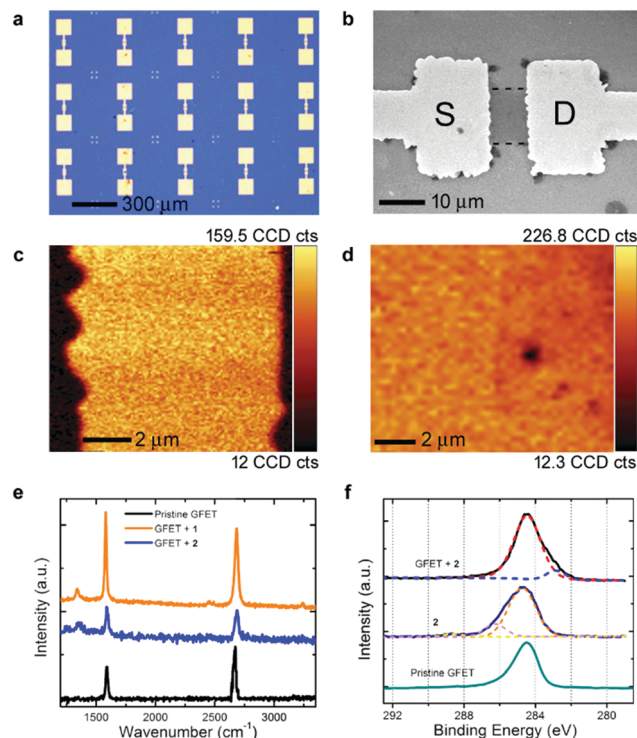

Fig. 2 (a) Optical image of arrays of GFETs. (b) SEM image of GFETs. (c) Raman mapping of pristine GFETs. (d) Raman mapping of GFETs functionalized with **1**. (e) Raman spectra of pristine GFETs (black) and GFETs functionalized with **1** and **2**. (f) XPS spectra of the pristine GFET, **2** and GFETs functionalized with **2** in the C1s region.

device characteristics. However, we note that the unique axial arrangement of the nitrate ligands with respect to the equatorial plane of L$_1$ in **1** or **2** plays a vital role in hindering such direct π–π interactions. Therefore, the charge-transfer to graphene is more likely to be mediated either through the nitrate ligands or by some other means (*vide infra*). Several control experiments were conducted to experimentally pinpoint the origin of such charge-transfer interactions. The doping characteristic of GFETs with both **1** and **2** is unchanged, irrespective of the electronic configuration of the lanthanide ions. Similarly, Ln(NO$_3$)$_3$·6H$_2$O (where Ln = La or Ce) and neat solvents were not observed to produce any change in electrical behaviour of GFETs. This implies that the central metal ion and the solvent do not directly participate in the interactions and are not responsible for the observed transport phenomenon (Fig. S6, ESI†). These observations unambiguously emphasise the importance of the unique structural arrangement of **1** and **2** for realising an electronic structure conducive for efficient n-doping of GFETs. This observation is in stark contrast to other existing literature reports where dopant-concentration and processing conditions dictate the final characteristics of GFETs.[7–12] Moreover, such dopant behaviour is achieved at single molecular, sub-monolayer surface coverage of the dopant (2.85 molecules per μm^2 for **1** and 0.61 molecules per μm^2 for **2**). Achieving such doping of graphene with inorganic macrocyclic complexes (**1** and **2**) is totally unprecedented in the literature and underlines the significance of the

structure–property correlation between the dopant and graphene. The nature of the interactions between the dopant and pristine GFETs upon functionalization and the associated changes in electronic structures are experimentally validated through micro-Raman spectroscopy and X-ray photoelectron spectroscopy (XPS, Fig. 2). Raman spectra of undoped GFETs (Fig. 2e) indicate a highly crystalline ordered phase with a prominent G-band ($1596\ cm^{-1}$) and 2D band ($2686\ cm^{-1}$).[19–23] The complete absence of the disordered D-band along with a I_{2D}/I_G ratio of 1.65 indicates monolayer, defect-free graphene which is confirmed through Raman spectral mapping (Fig. 2c, d and Fig. S7, ESI†).[22,23]

Upon adsorption of **1** or **2**, the Raman spectra exhibit prominent down-shifting of the G-peak along with simultaneous stiffening of the vibrational mode as observed by the lowering of FWHM ($22\ cm^{-1}$ for **1** and $14\ cm^{-1}$ for **2**, Fig. 2e). Furthermore, the magnitude of the shift in the G-band ($16\ cm^{-1}$ for **1** and $8\ cm^{-1}$ for **2**) and 2D-band is identical confirming the charge-transfer from the complex to graphene.[19,20] Importantly, the symmetry-forbidden D-band of graphene is minimized after doping, indicating weaker π–π interactions compared to conventional aromatic dopants (Fig. 2e).[24]

The absence of any intensity change in the G-band confirms the absence of any electron delocalization through π–π interactions. This is in excellent agreement with the theoretical finding that C–H···π interactions dominate the charge-transfer between **1** or **2** and graphene (*vide infra*). The massless fermions on graphene undergo ballistic transport leading to its ultra-high sensitivity towards any form of electronic perturbation.[25] This is critical in achieving uniform doping at sub-monolayer coverage over GFET channels that are at least 10^4 times larger than molecular dimensions, as confirmed through Raman spectral mapping carried out over the entire GFET (Fig. 2c–d).

These observations are substantiated through XPS. Pristine GFETs exhibit the characteristic peak at 284.4 eV, attributed to C1s of graphene. Similarly, the C1s of **2** exhibits the presence of the characteristic C1s peak (284.4 eV) along with a higher binding energy component at 286.3 eV originating from electron-deficient carbon (imino carbon) in the macrocyclic ligand of **2**. Upon doping, concomitant disappearance of this higher binding energy peak along with the appearance of a new peak at lower binding energy (282.8 eV) is observed in addition to the characteristic C1s peak (284.4 eV). The appearance of the low binding energy peak upon immobilization of **2** on GFETs indicates the charge-transfer mediated n-doping of GFETs by **2** (Fig. 2f).

To further confirm the realignment of energy levels upon doping of pristine GFETs with **2**, detailed Kelvin Probe Force Microscopy (KPFM) measurements were carried out (Fig. 3). The work-function (ϕ) of the pristine GFET and n-GFETs was estimated as

$$\phi_{sample} = \phi_{tip} - eV_{CPD}$$

where ϕ_{sample} and ϕ_{tip} refer to the work-function of the sample and the tip (respectively), e is the electronic charge and V_{CPD} represents the contact potential difference (CPD) between the sample and the tip. Consequently, the CPD estimated through
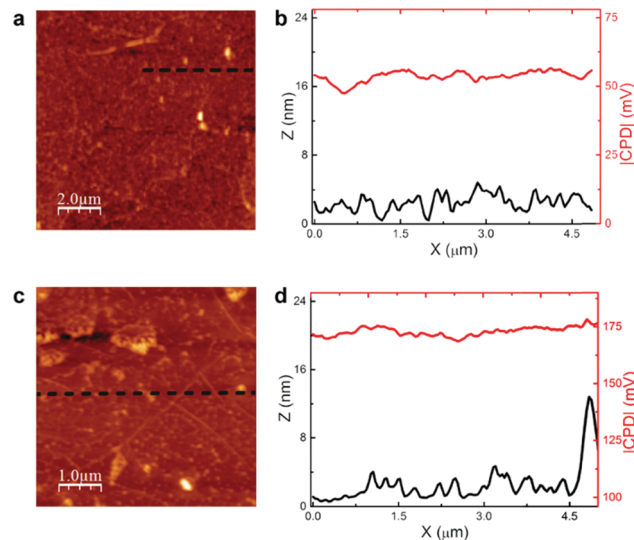

Fig. 3 (a) AFM topography of the channel region of the pristine GFET. (b) Corresponding height profile and the contact potential difference profile. (c) AFM topography of the channel region of GFETs functionalized with **2**. (d) Corresponding height profile and the contact potential difference profile.

these measurements exhibits a distinct increase from 61.5 mV for the pristine GFET to 188.3 mV for n-GFETs (Fig. 3b and d). The corresponding decrease in ϕ is estimated to be 0.2 eV upon doping, confirming the n-type doping of the GFET by **2**.[9] Finally, the topographical profile extracted from these measurements indicates an increase in the surface roughness, implying the immobilization of **2** on the GFET surface (Fig. 3a, c and Fig. S8, ESI†). Thus, the observed change in electrical properties of the pristine GFET upon doping is exclusively attributed to the dopants (**1** or **2**).

The unconventional, yet versatile doping approach (dispensing ultra-low volumes using femtojet) facilitates selective doping of devices at arbitrary locations with a high spatial precision and accuracy. Thus, we demonstrate that one specific micro-scale device with an area less than $0.05\ mm^2$ can be selectively doped in an ensemble of 150 devices covering an area of $\sim 20\ mm^2$, providing a spatial precision of $\sim 10^3$ (Fig. 2a and b).

To understand the molecular origin of the experimental observations, DFT calculations were performed using the Vienna *Ab initio* Simulation Package (VASP) using the PBE functional on complex **2** using supercells with 210 carbon atoms.[26–28] (See Fig. 4a and the ESI† for additional details). To study the adsorption of **1** and **2** on both pristine graphene and Stone–Wales defected graphene surfaces, we considered three different modes of adsorption for each with complexes interacting through two, one and zero nitrate groups (Fig. S9, ESI†). The relative energies of the optimized structures reveal that a favourable interaction exists between the graphene surface and the molecule with more exposed nitrate groups. Initial calculations were performed on pristine graphene (see the ESI† for details) and later possible Stone–Wales defects on graphene were taken into consideration based on the Raman spectra of pristine GFETs (Fig. 2e).
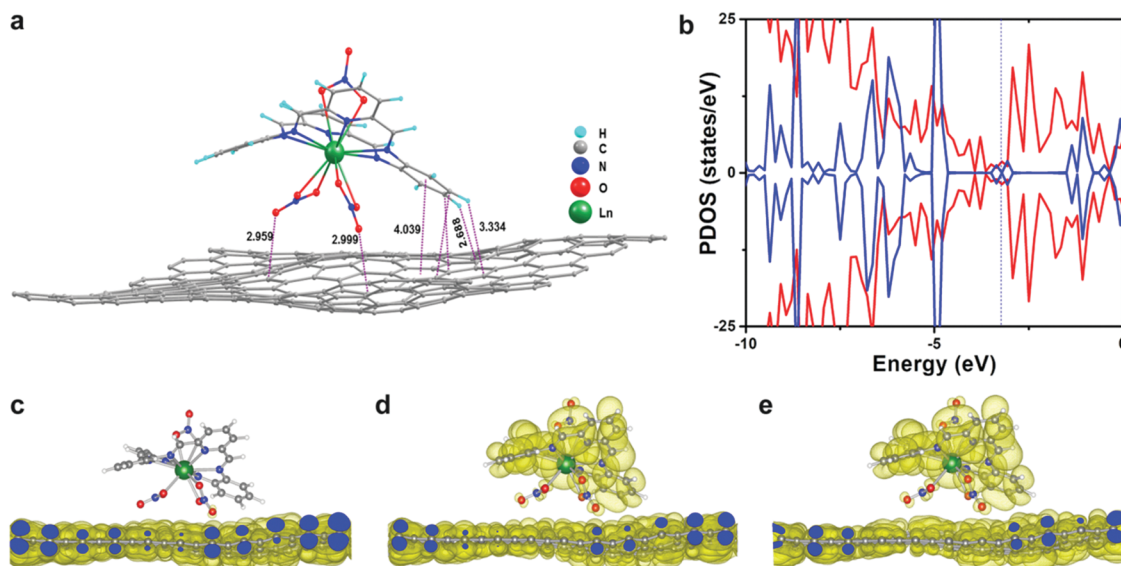
Fig. 4 (a) Optimized structure of **2** on Stone−Wales defected graphene (dotted lines show π−π and −CH···π interactions). Distances listed on panel a are in Angstroms. (b) Decomposed density of state (DOS) of Stone−Wales defected graphene before (red trace) and after (blue trace) the adsorption of **2**. (c−e) HOS, SOS, and LUS of **2** represented in panels, respectively.

In line with experimental observations, we have optimized **2** adsorbed on the Stone–Wales defected graphene surface (Fig. 4a). The binding energy ($E_{binding}$) computed here is −1880 meV suggesting favourable adsorption compared to the binding energies computed on the defect free graphene sheet earlier. Due to the presence of the five membered ring on the Stone–Wales defected surface, adsorption of **2** on the surface leads to significant structural distortion in the graphene substrate. In fact, the computed large $E_{binding}$ implies that n-doping of GFETs is an energetically favourable process that overcomes the influence of other p-dopants such as oxygen and water. This explains the stable n-doping of GFETs by **2**. A direct comparison of the $E_{binding}$ with other common dopants[7,29–36] is given in Fig. 5. The binding energies presented here are computed using a slightly different approach involving different functionals in comparison to **2**. In spite of this, the magnitude of the difference between **2** and other dopants is very significant implying that different exchange correlation functionals are unlikely to alter the trend. The absolute value of binding energies is provided here for comparative purposes. Such an Ashby plot indicates the unique solitary position occupied by **2** due to its strong binding energy in comparison to other common dopants. This further highlights the significance of employing air-stable inorganic molecular dopants to control the transport properties of graphene.

In particular, to avoid strong electrostatic repulsion with the molecules, the graphene surface tends to create a cavity around the molecule and this deformation of the surface is in fact favourable, as it is formed around one of the five membered rings. Due to this distortion, the molecule is found to approach closer to the surface with the closest atom–atom contact estimated to be 2.688 Å, much closer than that determined for the defect-free surface. Besides, the number of C–H···π and
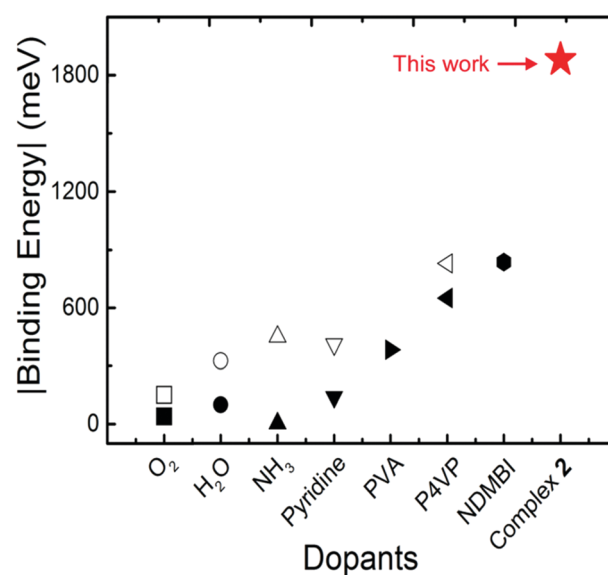

Fig. 5 Comparison plot of computed binding energies for different dopants (oxygen,[29,30] water,[31,32] ammonia,[33,34] pyridine,[7] polyvinyl alcohol (PVA),[35] poly-4-vinyl pyridine (P4VP),[7] 4-(1,3-dimethyl-2,3-dihydro-1H-(benzoimidazol-2-yl)phenyl)dimethylamine (NDMBI))[36] and complex **2** on the graphene surface.

π−π interactions enhanced, leading to stronger binding of the molecule on the surface, rationalizing the unchanged transport properties of GFETs for a prolonged time-frame. We would like to stress here that the optimized structure of the free standing Stone–Wales defected graphene layer maintains its planarity absolutely, while the distortion on the Stone–Wales defected graphene layer is introduced only upon adsorption of the molecule. From the computed density of states (DOS) plots (Fig. 4 and Fig. S10, ESI†), it can be observed that in the case

of graphene, the Dirac point and the Fermi level are coinciding. However, in the case of **2** adsorbed on Stone–Wales defected graphene, the Fermi level is found to be shifted towards the conduction band and the Dirac point is located around 0.26 eV below the Fermi level, rationalizing the observed n-type behaviour.

The decomposed DOS (Fig. 4b and Fig. S10, ESI†) shows significant contribution from complex states near the Fermi level along with the π^* states from graphene. The overlap between the complex states and graphene (π^*) states indicates the possible charge-transfer between the complex and the substrate which induces the observed n-type character of the composite. The band decomposed charge density iso-surface plots indicate that the highest occupied state (HOS) mainly results from the graphene π states and the single electron occupied state (SOS) and the lowest unoccupied state (LUS) are contributed by both the graphene surface and **2** (Fig. 4c–e). These plots reveal that the electron density obtained from the molecules particularly those of aromatic rings is found to possess depleted density as these groups are responsible for electron transfer from these parts of the ligand to the graphene surface.

Theoretical studies suggest that doping **2** on GFETs induces structural distortions of the graphene layer leading to a lowering of aromaticity of GFETs. This surface response upon adsorption is expected to take place slowly and this is one of the possible reasons why the as-fabricated device does not show strong n-type character immediately after doping, while a strong n-doped effect is visibly noticed after a few hours. This structural distortion presumably either facilitates the desorption of O_2/H_2O or prevents further adsorption of O_2/H_2O after achieving the n-type doping. The n-doping effect of **2** is unlikely to be overcome in either of these situations, as substantiated by measurements carried out at relative humidity levels of 90% (Fig. S4, ESI†) which further proves the strong interaction of **2** with GFETs.

The air-stability and unique doping techniques are combined to demonstrate complementary graphene inverters that are composed of the **1**-doped GFET providing the n-channel (n-GFET) and the pristine GFET acting as the p-channel (p-GFET, Fig. 6a). This is in contrast to other reports that utilize different dopants for achieving n- and p-characteristics.[7–14] In spite of this, we clearly observe complementary performance from both the channels. Positive V_{in} results in forward bias of the p-GFET leading to signalling between V_{DD} and the ground (Fig. 6b). Similarly, a negative bias provides inverter action by selectively opening the n-GFET channel (Fig. 6b). The maximum voltage-gain (V_{out}/V_{in}) achieved by such an inverter is 0.275 and is achieved at a V_{in} of −5 V and a V_{DD} of 2 V (Fig. 6c). However, the inverter exhibits hole dominated behaviour at lower V_{DD} (<1 V) resulting in a voltage gain of ~0.1 at a V_{in} of 5 V (Fig. 6c). This reinforces the ambipolarity of the device, thereby providing facile control over the gating characteristics with both types of charge carriers. The voltage gain obtained at a V_{DD} of 2 V (0.275) is four times higher than the obtained V_{DD} value of 0.5 V (0.067).
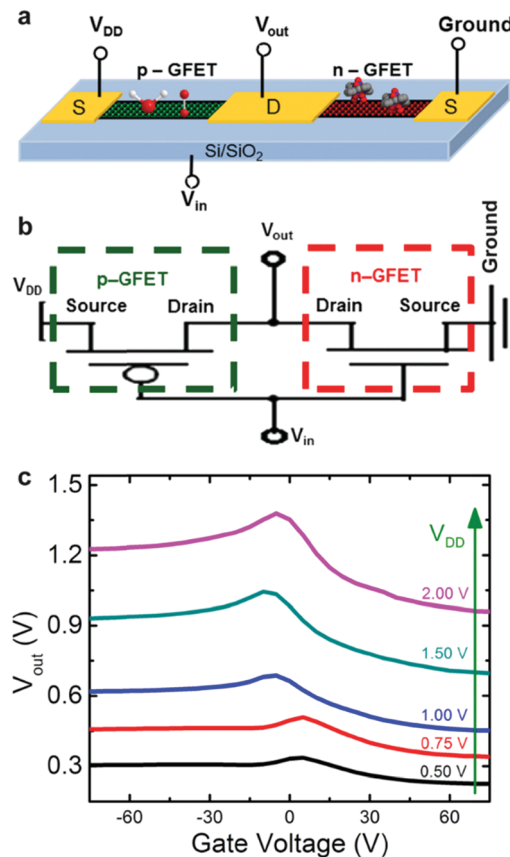

Fig. 6 (a and b) Schematic representation of the GFET inverter and its circuit diagram, respectively. (c) DC transfer characteristics of GFET inverters at different V_{DD}.

The n-doping being stronger and significant produces a stronger shift in the Dirac point, compared to the ambient p-doping, therefore resulting in the V_{in} of the inverter being located closer to the Dirac point of n-doped GFETs. Thus, the highest gain-point observed from such an inverter configuration is at −5 V with an offset of ~10 V. This value is among the highest reported for bottom-gated inverters.[7,10,12,13] In addition, the approach to realizing such hierarchically assembled inverters at arbitrary pre-defined positions provides a transformative opportunity towards realizing molecular-based electronic and spintronic devices.[37,38]

Conclusions

To conclude, we have demonstrated molecular level doping of graphene with **1** or **2** to realize n-type GFETs exhibiting extreme air-stability for over 10 months, without compromising their hole-electron transconductance (~ 7–8 μS), mobility (~ 900 cm^2 V^{-1} s^{-1}) and carrier concentration ($\sim10^{12}$ cm^{-2}). These performance indicators pertain to one of the highest levels achieved thus far, indicating the robustness of the approach and the importance of inorganic dopants. The importance of the molecular structure of the dopant towards realizing such performance is demonstrated through both experimental

and theoretical insights. The observed time dependent stabilization of stable n-doped GFETs was rationalized through detailed theoretical studies. Such investigations underline the importance of C–H$\cdots\pi$ interactions in tuning the electrical properties of two-dimensional materials, in contrast to the conventional knowledge of π–π based interactions. Finally, demonstration of inverters operational at 100 times lower power requirements (compared to existing reports) is expected to catalyse the practical realisation of molecular-based electronic devices.

Conflicts of interest

There are no conflicts to declare.

Acknowledgements

References

1 K. Kim, J.-Y. Choi, T. Kim, S.-H. Cho and H.-J. Chung, *Nature*, 2011, **479**, 338.

2 M. Y. Han, B. Özyilmaz, Y. Zhang and P. Kim, *Phys. Rev. Lett.*, 2007, **98**, 206805.

3 W. Bao, L. Jing, J. Velasco Jr, Y. Lee, G. Liu, D. Tran, B. Standley, M. Aykol, S. Cronin and D. Smirnov, *Nat. Phys.*, 2011, **7**, 948.

4 Y. Hao, L. Wang, Y. Liu, H. Chen, X. Wang, C. Tan, S. Nie, J. W. Suk, T. Jiang and T. Liang, *Nat. Nanotechnol.*, 2016, **11**, 426.

5 D. Wei, Y. Liu, Y. Wang, H. Zhang, L. Huang and G. Yu, *Nano Lett.*, 2009, **9**, 1752–1758.

6 V. Georgakilas, M. Otyepka, A. B. Bourlinos, V. Chandra, N. Kim, K. C. Kemp, P. Hobza, R. Zboril and K. S. Kim, *Chem. Rev.*, 2012, **112**, 6156–6214.

7 J. M. Yun, S. Park, Y. H. Hwang, E.-S. Lee, U. Maiti, H. Moon, B.-H. Kim, B.-S. Bae, Y.-H. Kim and S. O. Kim, *ACS Nano*, 2013, **8**, 650–656.

8 S. Kim, P. Zhao, S. Aikawa, E. Einarsson, S. Chiashi and S. Maruyama, *ACS Appl. Mater. Interfaces*, 2015, **7**, 9702–9708.

9 (a) W. Xu, T. S. Lim, H. K. Seo, S. Y. Min, H. Cho, M. H. Park, Y. H. Kim and T. W. Lee, *Small*, 2014, **10**, 1999–2005; (b) H. A. Becerril, J. Mao, Z. Liu, R. M. Stoltenberg, Z. Bao and Y. Chen, *ACS Nano*, 2008, **2**, 463–470.

10 Y. Choi, Q. Sun, E. Hwang, Y. Lee, S. Lee and J. H. Cho, *ACS Nano*, 2015, **9**, 4354–4361.

11 I. Jo, Y. Kim, J. Moon, S. Park, J. San Moon, W. B. Park, J. S. Lee and B. H. Hong, *Phys. Chem. Chem. Phys.*, 2015, **17**, 29492–29495.

12 P. Wei, N. Liu, H. R. Lee, E. Adijanto, L. Ci, B. D. Naab, J. Q. Zhong, J. Park, W. Chen and Y. Cui, *Nano Lett.*, 2013, **13**, 1890–1897.

13 F. Traversi, V. Russo and R. Sordan, *Appl. Phys. Lett.*, 2009, **94**, 150.

14 F. Xia, D. B. Farmer, Y.-M. Lin and P. Avouris, *Nano Lett.*, 2010, **10**, 715–718.

15 S. Ryu, L. Liu, S. Berciaud, Y.-J. Yu, H. Liu, P. Kim, G. W. Flynn and L. E. Brus, *Nano Lett.*, 2010, **10**, 4944–4951.

16 L. Britnell, R. Gorbachev, R. Jalil, B. Belle, F. Schedin, A. Mishchenko, T. Georgiou, M. Katsnelson, L. Eaves and S. Morozov, *Science*, 2012, **335**, 947–950.

17 H. Yang, J. Heo, S. Park, H. J. Song, D. H. Seo, K.-E. Byun, P. Kim, I. Yoo, H.-J. Chung and K. Kim, *Science*, 2012, **336**, 1140–1143.

18 W. J. Yu, Z. Li, H. Zhou, Y. Chen, Y. Wang, Y. Huang and X. Duan, *Nat. Mater.*, 2013, **12**, 246.

19 A. Das, S. Pisana, B. Chakraborty, S. Piscanec, S. Saha, U. Waghmare, K. Novoselov, H. Krishnamurthy, A. Geim and A. Ferrari, *Nat. Nanotechnol.*, 2008, **3**, 210.

20 A. C. Ferrari, J. Meyer, V. Scardaci, C. Casiraghi, M. Lazzeri, F. Mauri, S. Piscanec, D. Jiang, K. Novoselov and S. Roth, *Phys. Rev. Lett.*, 2006, **97**, 187401.

21 X. Li, W. Cai, J. An, S. Kim, J. Nah, D. Yang, R. Piner, A. Velamakanni, I. Jung and E. Tutuc, *Science*, 2009, **324**, 1312–1314.

22 Y. Gui, H. Sun, H. Yan, H. Wang, Y. Zhang, X. M. Song and R. Jia, *Solid State Commun.*, 2017, **264**, 31–34.

23 C. Bautista-Flores, R. Sato-Berrú and D. Mendoza, *Mater. Res. Express*, 2018, **6**, 015601.

24 M. J. Deka and D. Chowdhury, *J. Phys. Chem. C*, 2016, **120**, 4121–4129.

25 K. S. Novoselov, A. K. Geim, S. V. Morozov, D. Jiang, Y. Zhang, S. V. Dubonos, I. V. Grigorieva and A. A. Firsov, *Science*, 2004, **306**, 666–669.

26 G. Kresse and J. Furthmüller, *Comput. Mater. Sci.*, 1996, **6**, 15–50.

27 G. Kresse and J. Furthmüller, *Phys. Rev. B: Condens. Matter Mater. Phys.*, 1996, **54**, 11169.

28 J. P. Perdew, K. Burke and M. Ernzerhof, *Phys. Rev. Lett.*, 1996, **77**, 3865.

29 V. Blechta, K. A. Drogowska, V. Vales and M. Kalbac, *J. Phys. Chem. C*, 2018, **122**, 21493–21499.

30 F. R. Bagsican, A. Winchester, S. Ghosh, X. Zhang, L. Ma, M. Wang, H. Murakami, S. Talapatra, R. Vajtai and P. M. Ajayan, *Sci. Rep.*, 2017, **7**, 1774.

31 M. Gordillo and J. Marti, *J. Phys.: Condens. Matter*, 2010, **22**, 284111.

32 J. Ma, A. Michaelides, D. Alfe, L. Schimka, G. Kresse and E. Wang, *Phys. Rev. B: Condens. Matter Mater. Phys.*, 2011, **84**, 033402.

33 S. Böttcher, H. Vita, M. Weser, F. Bisti, Y. S. Dedkov and K. Horn, *J. Phys. Chem. Lett.*, 2017, **8**, 3668–3672.

34 F. Ma, Y. Jiao, Y. Gu, A. Bilic, Y. Chen, Z. Chen and A. Du, *Sci. Rep.*, 2016, **6**, 33810.

35 Z. W. Ulissi, J. Zhang, V. Sresht, D. Blankschtein and M. S. Strano, *Langmuir*, 2014, **31**, 628–636.

36 P. A. Denis and F. Iribarne, *J. Phys. Chem. C*, 2015, **119**, 15103–15111.

37 C. Cervetti, A. Rettori, M. G. Pini, A. Cornia, A. Repollés, F. Luis, M. Dressel, S. Rauschenbach, K. Kern and M. Burghard, *Nat. Mater.*, 2016, **15**, 164.

38 A. Candini, S. Klyatskaya, M. Ruben, W. Wernsdorfer and M. Affronte, *Nano Lett.*, 2011, **11**, 2634–2639.